Preparation of Sr_2CeO_4 Blue Phosphor Particles and Rare Earth (Eu, Ho, Tm, or Er)-Doped Sr_2CeO_4 Phosphor Particles, Using an Emulsion Liquid Membrane System

Takayuki Hirai* and Yusuke Kawamura

Research Center for Solar Energy Chemistry, and Division of Chemical Engineering, Graduate School of Engineering Science, Osaka University, Toyonaka, Osaka 560-8531, Japan

Received: March 15, 2004; In Final Form: June 4, 2004

Sr_2CeO_4 blue phosphor particles were prepared with an emulsion liquid membrane (ELM, water-in-oil-in-water (W/O/W) emulsion) system, which could be utilized as a microreactor for the preparation of size- and morphology-controlled fine particles. In the ELM system, Sr^{2+} and Ce^{3+} ions were extracted from the external water phase by extractant (cation carrier, bis(2-ethylhexyl)phosphoric acid) and were stripped into the internal water phase, containing oxalic acid solution, to form the submicrometer-sized composite Sr−Ce oxalate particles, which were much smaller than those obtained in a homogeneous aqueous solution. Calcination of the precursor oxalate particles obtained in the ELM system produced submicrometer-sized Sr_2CeO_4 particles, which showed a charge-transfer (CT) emission at 467 nm (λ_{ex} = 254 nm). The photoluminescence properties of rare earth-doped Sr_2CeO_4 (Sr_2CeO_4:Ln^{3+}; Ln = Eu, Ho, Tm, or Er) were also investigated, and the characteristic emissions corresponding to doped rare earth ions, effected by energy transfer from the triplet excited state of MLCT (metal-to-ligand charge transfer) state for Sr_2CeO_4 (sensitizer) to the rare earth ions (activators), were observed.

Introduction

An emulsion liquid membrane (ELM, water-in-oil-in-water (W/O/W) emulsion) system has been studied for the separation of metals, in which the metal ions are extracted from the external water phase into the organic membrane phase, where they are then stripped and concentrated into the internal water phase. Such an internal water phase obtained via the ELM system has been found to be capable of being used as a "microreactor" for the preparation of size-controlled and morphology-controlled fine particles due to the restricted reaction area of the internal water droplets. This microreactor is also interesting because it provides a hydrophobic environment and templating effect at the interface between the organic membrane phase and internal water phase. The particles, having different characteristics from those obtained in bulk (homogeneous) aqueous solutions, are therefore obtained in the ELM system, such as submicrometer-sized spherical rare earth oxalate particles[1−3] and calcium carbonate particles having vaterite structure,[4] by the reaction of oxalic acid or sodium carbonate fed in the internal water phase and the metal ions fed in the external water phase and then transported into the internal phase. This methodology is successfully extended to the preparation of composite oxalate particles by feeding two or more different metal ions into the external water phase. The resulting composite oxalate particles give oxide particles, such as $SrPbO_3$ and Sr_2PbO_4,[5] Co and Ni ferrites,[6] Y_2O_3:Eu^{3+},[7] Gd_2O_3:Eu^{3+},[8] Y_2O_3:Yb^{3+},Er^{3+},[9] and Gd_2O_3:Yb^{3+},Er^{3+},[10] by calcination. It was found that Sr oxalate precipitates more easily in the internal water phase than in the homogeneous aqueous solution.[5]

It is difficult to find a suitable blue phosphor because a wide band gap energy is needed to obtain blue emission. In a practical use, Eu^{2+}-activated $BaMgAl_{10}O_{17}$ (BAM) is employed, which shows blue emission originated from 4f−5d transition.[11] A critical problem of this material is that a very high calcination temperature is needed to prepare a pure BAM.[12] Sulfide phosphors, for example, ZnS:Ag, are also utilized as blue phosphors, but these materials tend to degrade under electron excitation.[13]

Recently, Danielson et al. identified that a new oxide-based blue phosphor (Sr_2CeO_4) exhibits blue-white luminescence due to the charge transfer (CT) mechanism by a combinatorial method.[14] Several researchers also investigated the detailed emission mechanism of this phosphor.[15−17] Sr_2CeO_4 is a phosphor with 100% active center concentration, thus all CeO_6 octahedra may be considered as fluorescent centers and quantum efficiency is very high. Sr_2CeO_4 might also act as a sensitizer to transfer the absorbed energy to the dopants (activator), because of the possibility of energy transfer from Sr_2CeO_4 to the dopant ions. However, only a few papers have been published about the doping of rare earth ions in Sr_2CeO_4.[17,18]

In the present work, we prepared Sr_2CeO_4 fine particles using an ELM system. Sr−Ce oxalate particles were prepared in the ELM system containing D2EHPA (bis-2(ethylhexyl)phosphoric acid) as an extractant (cation carrier) to transport Sr and Ce ions from the external water phase into the internal water phase. The resulting oxalate particles prepared in the ELM system were calcined to obtain Sr_2CeO_4, and their size, morphology, and luminescence properties were investigated. We also investigated the luminescence properties of rare earth-doped Sr_2CeO_4, Sr_2CeO_4:Ln^{3+} (Ln = Eu, Ho, Tm, or Er).

Experimental Section

Bis(2-ethylhexyl)phosphoric acid (D2EHPA, supplied by Daihachi Chemical Industry Co., Ltd., Osaka) was used as the extractant after purification, and sorbitan sesquioleate (Span 83,

* Author to whom correspondence should be addressed. Phone: +81-6-6850-6270. Fax: +81-6-6850-6273. E-mail: hirai@cheng.es.osaka-u.ac.jp.

10.1021/jp040220p CCC: $27.50
Published on Web 07/31/2004

supplied by Tokyo Kasei Kogyo Co., Ltd., Tokyo) was used as the surfactant. Strontium nitrate ($Sr(NO_3)_2$), cerium nitrate hexahydrate ($Ce(NO_3)_3 \cdot 6H_2O$), strontium carbonate ($SrCO_3$), oxalic acid, and acetone were supplied by Wako Pure Chemical Industries, Ltd. Cerium oxide (CeO_2) was supplied by Nippon Yttrium Co., Ltd.

The oxalate particles were prepared via a procedure similar to that reported previously.[5,6] The internal water phase (0.5 mol/L of oxalic acid) and the organic membrane phase (kerosene containing 0.5 mol/L of D2EHPA and 5 wt % Span 83) were mixed at a volume ratio of 1:1, and were emulsified mechanically with a homogenizer (12 000 rpm). The resulting W/O emulsion (10 mL) was then added to the external water phase (50 mL of $Sr(NO_3)_2$ and $Ce(NO_3)_3$ aqueous solution) and the solution was stirred vigorously with a magnetic stirrer (500 rpm) to form a W/O/W emulsion. The total metal concentration of the external aqueous solution was always fixed at 4 mmol/L, and the molar ratio of concentrations in the feed external solution, $(Sr/Ce)_f$, was varied. For the preparation of rare earth ($Ln^{3+} = Eu^{3+}$, Ho^{3+}, Tm^{3+}, or Er^{3+})-doped composite oxalate particles, the respective rare earth nitrate ($Ln(NO_3)_3$) or chloride ($LnCl_3$) was added to the external water phase, with the molar ratio of concentrations, $(Ln/(Ln+Ce))_f$ and $(Sr/(Ln+Ce))_f$, fixed at 0.01 and 4, respectively, but $(Eu/(Eu+Ce))_f$ was varied in the case of Eu^{3+} to investigate the effect of the concentration of dopant ion. After being stirred for 1 h, the W/O emulsion was then separated from the external aqueous solution and demulsified by adding 50 mL of acetone. The particles formed in the water droplets were separated by centrifuge, washed with acetone twice, and dried at room temperature. The oxalate particles were finally calcined in air, at 1223 or 1273 K for 2 h, to obtain Sr_2CeO_4.

Sr_2CeO_4 particles were also prepared via a solid-state method for comparison purposes. $SrCO_3$ and CeO_2 were used as starting materials, and then mixed stoichiometrically and homogenized in an agate mortar. This homogenized mixture was calcined at 1273 K for 72 h with two intermediate regrindings.

The composite oxalate particles and oxide particles were characterized by means of scanning electron microscopy (SEM, Hitachi S-5000 and S-2250N), powder X-ray diffraction (XRD, Philips PW-3050), and thermogravimetric/differential thermal analysis (TG-DTA, Shimadzu TG-DTA50). To determine the molar composition, $(Sr/Ce)_p$, of the composite oxalate particles, the particles were dissolved in 1 mol/L of HCl and the metal concentrations were measured by using an ICP-AES (Nippon Jarrell-Ash ICAP-575 Mark II). To determine the metal concentrations in each phase of the ELM system, the separated W/O emulsion was demulsified electrically and the organic phase was then stripped with 1 mol/L of HCl. The metal concentrations both in the external water phase and in the resulting stripping solutions were determined by ICP-AES. The metal concentration in the internal water phase was calculated by mass balance. The photoluminescence spectra of the particles were measured with a spectrofluorometer (JASCO FP-777, Xe lamp). Lifetime measurements were carried out with a fluorescence lifetime spectrometer (Photon Technology International PTI-2100, 75 W Xe flash lamp, pulse width ~ 5 μs).

Results and Discussion

Preparation and Characterization of Sr−Ce Composite Oxalate Particles Prepared in the ELM System. SEM images of Sr oxalate, Ce oxalate, and composite Sr−Ce oxalate particles prepared in the ELM system at $(Sr/Ce)_f = 4$ are shown in Figure 1. Irregular-shaped particles were obtained for the Sr oxalate,[5]

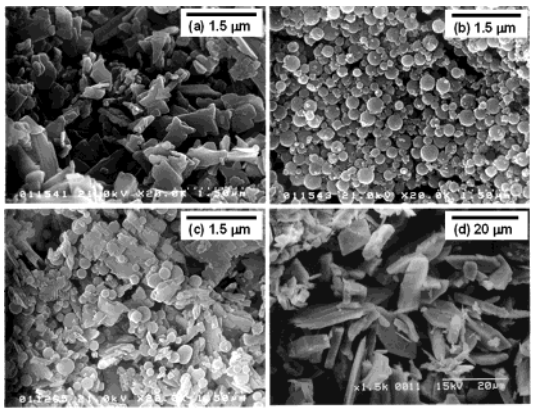

Figure 1. SEM images for (a) Sr oxalate, (b) Ce oxalate, and (c) composite Sr−Ce oxalate particles prepared at $(Sr/Ce)_f = 4$ in the ELM system, and (d) composite Sr−Ce oxalate particles prepared at $(Sr/Ce)_f = 6$ in homogeneous aqueous solution.

and spherical particles were obtained for the Ce oxalate as in the case with phosphonic acid ester extractant.[1] In the composite Sr−Ce system, both the irregular-shaped particles and spherical particles were observed, which seemed to be a mixture of Sr oxalate and Ce oxalate. For comparison, the SEM image for the composite Sr−Ce oxalate particles obtained in a homogeneous aqueous solution by adding a 0.1 mol/L of metal nitrate solution ($(Sr/Ce)_f = 6$) to a 0.5 mol/L of oxalic acid solution is shown in Figure 1d. The irregular-shaped particles greater than 20 μm in size were obtained in the homogeneous aqueous solution. The ELM system is therefore effective in controlling the particle size.

Figure 2 shows the time-course variations for the mole percent compositions of the metal ions in the external water phase, in the organic membrane phase, and in the internal water phase of the ELM system. The organic membrane phase does not contain appreciable amounts of Sr^{2+} and Ce^{3+} after 60 min, indicating that the metal ions extracted from the external water phase are effectively transported into the internal water phase. Although Ce^{3+} was transported into the internal water phase almost completely within 60 min, 20% of Sr^{2+} remained in the external water phase even after 120 min of stirring. The transport behavior for Ce^{3+} in the composite Sr−Ce system was similar to that in the single Ce system. In contrast, the transport of Sr was slightly decreased in the composite Sr−Ce system from that in the single Sr system. The final molar ratio of the two metals transported into the internal water phase was therefore slightly different from the feed molar ratio, indicating that the transport of Sr probably was affected by the presence of Ce.[19]

The effect of feed molar ratio of Sr^{2+} and Ce^{3+} in the external water phase, $(Sr/Ce)_f$, on the molar composition of the resulting oxalate particles, $(Sr/Ce)_p$, was investigated to obtain stoichiometric Sr_2CeO_4 particles. The results shown in Figure 3 indicate the appropriate feed composition is $(Sr/Ce)_f = 3$ to achieve $(Sr/Ce)_p = 2$. The values of $(Sr/Ce)_p$ obtained in the ELM system are much greater than those obtained in the homogeneous aqueous solution. This indicates that the yield of Sr oxalate is much greater in the ELM system than in the homogeneous system, as reported previously.[5] This is probably caused by the hydrophobic property of the interfacial reaction area between the organic membrane phase and internal water phase, where the solubility of Sr oxalate may be smaller than that in bulk aqueous solutions.

Calcination of Composite Sr−Ce Oxalate Particles. Figure 4 shows the TG-DTA curves for the composite Sr−Ce oxalate particles prepared in the ELM system. The TG curve showed

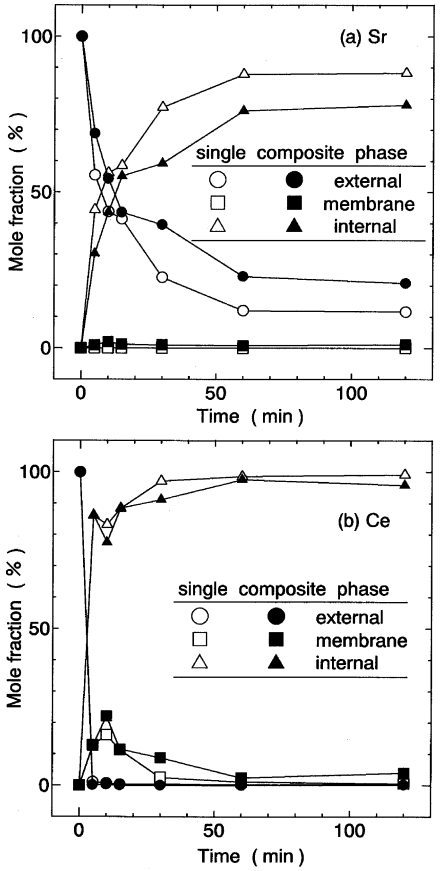

Figure 2. Time-course variations for the mole fraction composition of (a) Sr and (b) Ce ions in the external water phase, organic membrane phase, and internal water phase of the ELM in the single and composite systems at $(Sr/Ce)_f = 4$. The mole fraction in the initial external water phase is set as 100%.

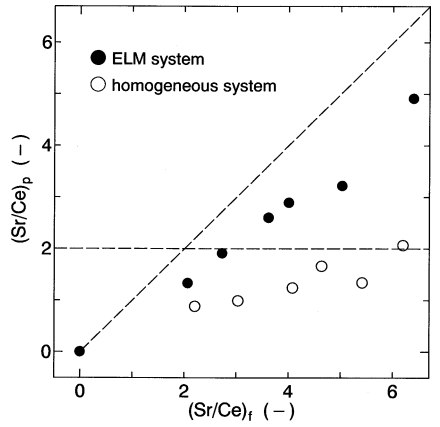

Figure 3. Relationship between the feed molar ratio, $(Sr/Ce)_f$, and the composition of the particles, $(Sr/Ce)_p$, for the particles prepared in the ELM system and homogeneous aqueous solution.

three steps in this measurement and weight loss finished around 1150 K. Endothermic peaks appeared at around 326, 433, and 1130 K and exothermic peaks also appeared at 609 and 714 K. These peaks correspond to the formation of dehydrate oxalate (first two peaks), CeO_2 via $Ce_2O_2CO_3$ (609 K), and $SrCO_3$ (714 K), respectively, and the last peak at 1130 K might correspond to the decomposition of $SrCO_3$ and formation of Sr_2CeO_4. On the basis of the result from the TG-DTA analysis, the oxalate particles prepared in the ELM system were calcined at 1273 K for 2 h.

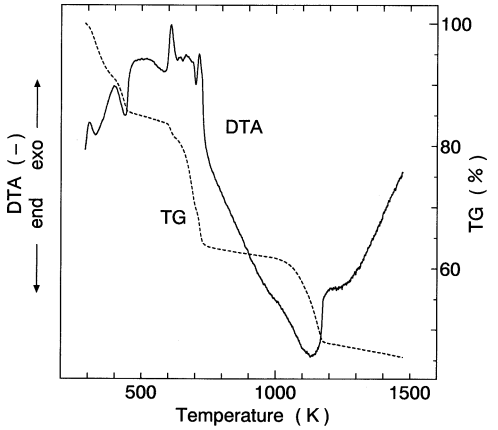

Figure 4. TG-DTA curves for composite Sr−Ce oxalate particles prepared in the ELM system at $(Sr/Ce)_f = 4$.

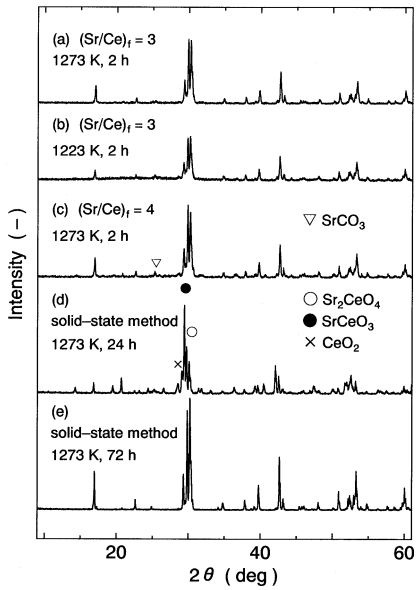

Figure 5. X-ray diffraction patterns for composite Sr−Ce oxide particles obtained by calcination of composite oxalate particles prepared in the ELM system (a: $(Sr/Ce)_f = 3$, 1273 K for 2 h; b: $(Sr/Ce)_f = 3$, 1223 K for 2 h; c: $(Sr/Ce)_f = 4$, 1273 K for 2 h) and by the solid-state method (d: 1273 K for 24 h; e: 1273 K for 72 h, with two intermediate regrinding).

When $(Sr/Ce)_f = 2$ was employed, the $SrCeO_3$ phase was mainly obtained, because the composition of the precursor oxalate particles ($(Sr/Ce)_p$) was much smaller than 2 (Figure 2). The precursor oxalate particles were therefore prepared at $(Sr/Ce)_f \geq 3$. Figure 5 shows XRD patterns of the composite Sr−Ce oxide particles obtained via the calcination of the precursor composite oxalate particles prepared in the ELM system at $(Sr/Ce)_f = 3$ or 4, together with those of composite oxide particles prepared by the solid-state method. The calcination of the oxalate particles prepared at $(Sr/Ce)_f = 3$ gave a single phase of the Sr_2CeO_4 at the calcination temperature of 1273 K (Figure 5a), and even at 1223 K (Figure 5b). At $(Sr/Ce)_f = 4$, the resulting particles were mainly Sr_2CeO_4 but also contained the $SrCO_3$ phase as a minor phase (Figure 5c). On the contrary, the particles obtained via the solid-state method calcined at 1273 K for 24 h contained several phase such as Sr_2CeO_4, $SrCeO_3$, and CeO_2 (Figure 5d). To obtain pure Sr_2CeO_4 phase via the solid-state method, repeated grinding and subsequent calcination at 1273 K for 24 h for three times were required (Figure 5e). Masui et al. prepared submicrometer-sized Sr_2CeO_4 particles by calcination of composite Sr−Ce carbonate

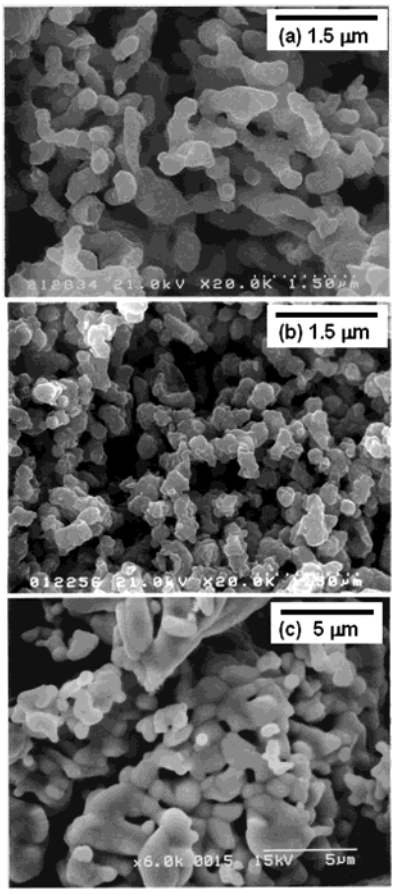

Figure 6. SEM images for Sr_2CeO_4 particles obtained by calcination of composite oxalate particles prepared in the ELM system ($(Sr/Ce)_f = 4$) at 1273 K for (a) 2 h and (b) 6 h and (c) by the solid-state method.

particles, prepared via the coprecipitation method, at 1373 K for 2 h.[20] Compared to the solid-state method and the previously reported method, we have therefore succeeded in synthesizing Sr_2CeO_4, via calcination for shorter heating time and/or at lower temperature, by using the ELM system. This probably is achieved by reducing the particle size of precursor composite oxalate particles.

Oxalate particles are well-known as excellent precursors to obtain oxide particles by calcination. Jiang et al. reported on the preparation of Sr_2CeO_4 from composite Sr−Ce oxalate particles obtained by chemical coprecipitation.[21] The size of the particles, however, increased up to 2−6 μm with increasing the calcination temperature up to 1673 K. On the contrary, it is expected to control the size and morphology of the oxalate and oxide particles by using the ELM system. Figure 6 shows SEM images for the Sr_2CeO_4 particles obtained by calcination of the composite oxalate particles prepared in the ELM system and by the solid-state method. The oxide particles prepared in the ELM system were slightly sintered (Figure 6a), because alkaline earth metals, viz. Ba, Sr, Ca, and Mg, are relatively ductile metals.[12,22] The main component of the particles, however, still maintained their submicrometer size. On the contrary, much larger particles with irregular shape were obtained by the solid-state method (Figure 6c).

A serious problem for the Sr_2CeO_4 particles is that Sr_2CeO_4 phase is not very stable. Park et al. reported that the Sr_2CeO_4 prepared by the solid-state method was decomposed into $SrCO_3$ and an unknown phase when exposed to air for a long time.[16] However, the details of a series of decomposition steps of Sr_2CeO_4 have not been revealed. Figure 7 shows the time course

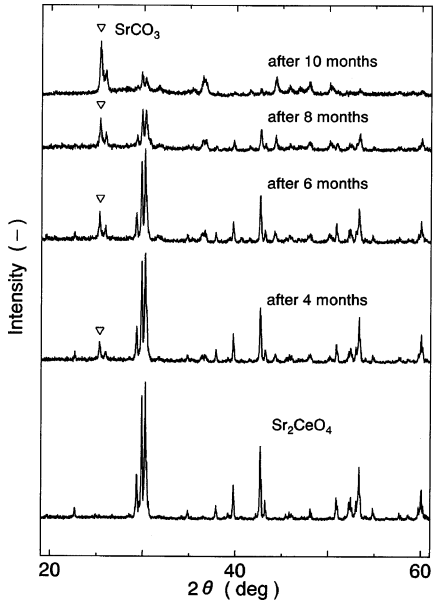

Figure 7. Time-course variation for the X-ray diffraction pattern of Sr_2CeO_4 obtained by calcination of composite oxalate particles prepared in the ELM system ($(Sr/Ce)_f = 3$) at 1273 K for 2 h.

variation of the XRD patterns for oxide particles prepared in the ELM system. Although the Sr_2CeO_4 phase remained for 6 months, the $SrCO_3$ phase appeared gradually. Finally, the Sr_2CeO_4 phase disappeared completely and decomposed into $SrCO_3$ and an unknown phase after 10 months, and the blue-white luminescence originating from $Ce^{4+}-O^{2-}$ CT also diminished. This decomposition occurs in air, and may be caused by the reaction of Sr_2CeO_4 with CO_2. To avoid this problem, therefore, surface modification to protect Sr_2CeO_4 against air and/or CO_2 may be effective for practical use.

Luminescent Properties of Sr_2CeO_4 Particles. Sr_2CeO_4 is one of the few materials which show CT luminescence originated from $Ce^{4+}-O^{2-}$ CT.[14] Such CT luminescence cannot be observed for other trivalent rare-earth ions except for Yb^{3+}.[23,24] The emission spectra for the Sr_2CeO_4 particles measured at room temperature are shown in Figure 8. The broad blue-white emission peak around 467 nm was observed at $\lambda_{ex} = 254$ nm as well as $\lambda_{ex} = 355$ nm regardless of the preparation method and condition. Sr_2CeO_4 is also known as the blue phosphor with a long lifetime due to the CT emission from the triplet excited state.[15] The photoexcitation occurs from the ground state to t_{1g}-f CTS (charge transfer state), where t_{1g} is the molecular orbital of the ligand in 6-fold oxygen coordination and f is the lowest excited CTS of the Ce^{4+} ion.[17,18] A fast relaxation to the lower triplet excited state (high spin excited state) then occurs.[15,17] This change of the spin orientation is likely to give the long lifetime because of the spin-forbidden transition. The emission around 467 nm is attributable to the transition from the MLCT (metal-to-ligand charge transfer) state to the ground state.[17] Figure 9a shows the luminescence decay curves for Sr_2CeO_4 prepared in the ELM system. A decay time measured at room temperature and at $\lambda_{ex} = 280$ nm was determined to be 42 μs for Sr_2CeO_4, which was comparable to that reported previously.[14,15] A similar luminescence decay curve was also obtained at $\lambda_{ex} = 340$ nm (29 400 cm^{-1}), indicating that the long lifetime of Sr_2CeO_4 is attributable to the long lifetime of the triplet state of the MLCT state.[15,17]

The particles prepared in the ELM system at $(Sr/Ce)_f = 3$ showed lower emission intensity than the particles prepared by the solid-state method. The emission intensity may be affected

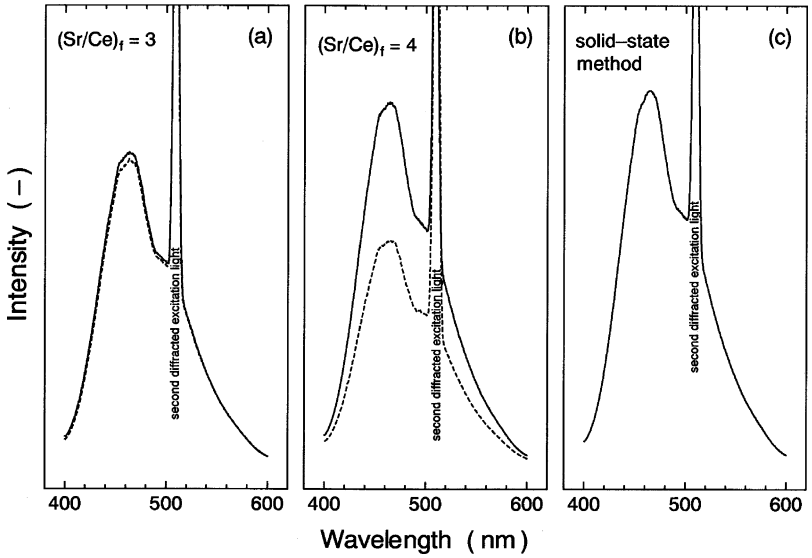

Figure 8. Photoluminescence spectra for Sr_2CeO_4 particles obtained by calcination of composite oxalate particles prepared in the ELM system (a: $(Sr/Ce)_f = 3$; b: $(Sr/Ce)_f = 4$) at 1273 K for 2 h (dotted lines) and 6 h (solid lines) and (c) by the solid-state method. $\lambda_{ex} = 254$ nm.

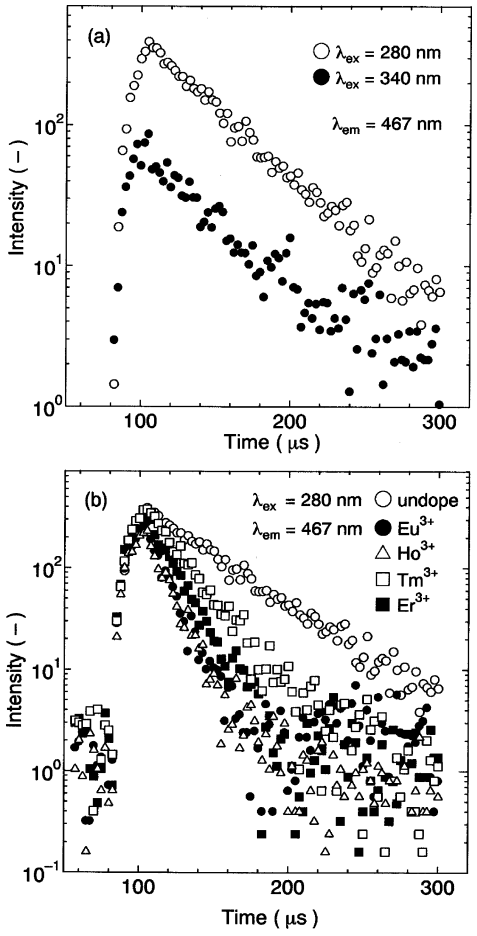

Figure 9. Luminescence decay curves for Sr_2CeO_4 and $Sr_2CeO_4:Ln^{3+}$ particles prepared in the ELM system measured at room temperature monitoring the emission at 467 nm: (a) Sr_2CeO_4 at $\lambda_{ex} = 280$ and 340 nm and (b) Sr_2CeO_4 and $Sr_2CeO_4:Ln^{3+}$ at $\lambda_{ex} = 280$ nm.

by the number of oxygen defects, which decrease the luminescence intensity.[15] It was found that the emission intensity of the particles prepared at $(Sr/Ce)_f = 3$ scarcely varied even though the calcination time was extended to 6 h, but the intensity remarkably increased for particles prepared at $(Sr/Ce)_f = 4$ with calcination for 6 h, and was comparable to that for the particles

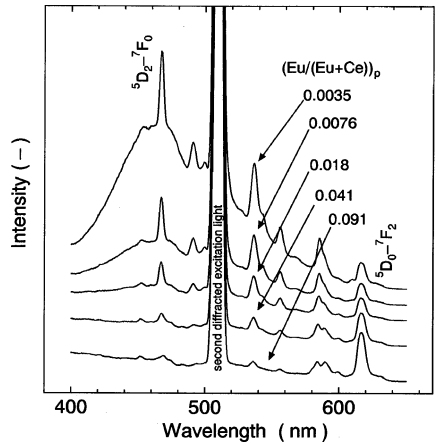

Figure 10. Effect of Eu content on the photoluminescence spectra of $Sr_2CeO_4:Eu^{3+}$ particles prepared in the ELM system. $\lambda_{ex} = 254$ nm.

obtained by the solid-state method. In addition, the morphology of the particles hardly changed after 6 h of calcination, as shown in Figure 6b. The additional Sr oxalate might act as a flux and the resulting Sr compounds cover the surface of the Sr_2CeO_4 particles to decrease the oxygen defects effectively, because Sr oxalate particles sinter easily at 1273 K.

Luminescent Properties of Rare Earth-Doped Sr_2CeO_4 Particles. The emission behavior of the Eu^{3+}- or Sm^{3+}-doped Sr_2CeO_4 particles, in which the CeO_6 groups act as sensitizers, i.e., energy donors, and the Eu^{3+} or Sm^{3+} ions act as activators, i.e., energy acceptors, was reported.[17]

The $Sr_2CeO_4:Eu^{3+}$ particles prepared with use of the ELM system showed white emission at molar composition of the particles $(Eu/(Eu+Ce))_p = 0.0076$ and red emission gradually increased by increasing the $(Eu/(Eu+Ce))_p$ value. Actually, the emission spectrum for the $Sr_2CeO_4:Eu^{3+}$ particles at $\lambda_{ex} = 254$ nm varied considerably with the concentration of Eu^{3+}, as shown by Figure 10. When the Eu^{3+} concentration was low, the broad emission band originated from Sr_2CeO_4 itself and the Eu^{3+} emission lines in the blue and green regions were observed. On the contrary, at the higher Eu^{3+} concentration, the broad emission band disappeared and the Eu^{3+} emission lines in the red region gradually appeared at around 610 nm. The most interesting result is that the emission line assigned to the $^5D_2$-$^7F_0$ transition in Eu^{3+} appears in the blue region at around 467

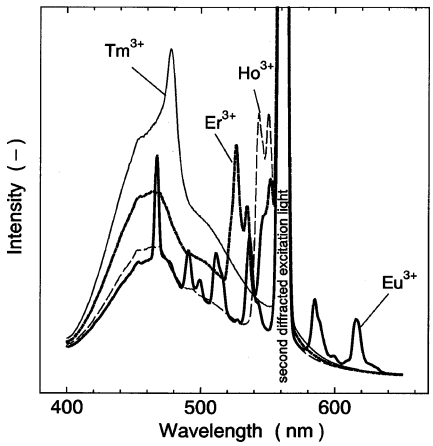

Figure 11. Photoluminescence spectra of Sr_2CeO_4:Eu^{3+}, Sr_2CeO_4:Ho^{3+}, Sr_2CeO_4:Tm^{3+}, and Sr_2CeO_4:Er^{3+} particles prepared in the ELM system. $\lambda_{ex} = 280$ nm.

nm at low concentrations of Eu^{3+}. Generally, this emission is hardly observed when Eu^{3+} is doped in other oxide hosts, since the general oxide host lattice has higher photon energy and thus a nonradiative energy loss from a higher ^5D state due to multiphonon relaxation occurs.[25] The relative intensities of the $^5D_2$-$^7F_0$ and $^5D_0$-$^7F_2$ transition were varied with increasing Eu^{3+} concentration in the particles, probably because the cross-relaxation between $^5D_2$-^5D_J ($2 > J \geq 0$) and $^7F_0$-$^7F_{J'}$ ($6 > J' > 0$) is likely to be accelerated by increasing the Eu^{3+} concentration.

When Ho^{3+}, Tm^{3+}, or Er^{3+} was doped, the emission peaks peculiar to these ions appeared under similar excitation conditions ($\lambda_{ex} = 280$ nm). As shown in Figure 11, Ho^{3+} shows green emission assigned to the ($^5S_2$, $^5F_4$)-$^5I_8$ transition, Tm^{3+} shows only blue emission assigned to the $^1G_4$-$^3H_6$ transition, and Er^{3+} shows only ($^2H_{11/2}$, $^4S_{3/2}$)-$^4H_{15/2}$ transition in the green region without emission in the red ($^4F_{9/2}$-$^4I_{15/2}$) region. The energy diagram for Sr_2CeO_4:Ln^{3+} (Ln = Eu, Sm, and Yb) was proposed by Nag et al.[17] They supposed that the energy transfers from t_{1g}-f CTS to Ln^{3+}-O^{2-} CTS and then emission originating from every Ln^{3+} ion occurs. In the case of Tm^{3+}, therefore, if the energy transfer from t_{1g}-f CTS to Tm^{3+}-O^{2-} CTS occurs, the emission originating from the $^1D_2$-$^3F_4$ or $^3P_0$-$^3F_3$ transition should appear between 450 and 460 nm similarly to the cases of Y_2O_3:Tm^{3+} [26] and $SrHfO_3$:Tm^{3+}.[27] In our experiment, however, only a sharp emission peak around 477 nm originating from the $^1G_4$-$^3H_6$ transition was observed, as shown in Figure 11. This emission was also observed when the Sr_2CeO_4:Tm^{3+} particles were excited at $\lambda_{ex} = 355$ nm (28 200 cm^{-1}). $^1D_2$ and $^3P_0$ states lie around 27 500 and 35 000 cm^{-1}, respectively, which are lower than the t_{1g}-f CTS and higher than the MLCT state for Sr_2CeO_4, as schematically shown by the energy diagram (Figure 12). In addition, Tm^{3+}-O^{2-} CTS lies higher than 40 000 cm^{-1}, even when the host material is $SrHrO_3$ having a relatively low CTS of Tm^{3+}.[27] These results suggest the emission mechanism for Sr_2CeO_4:Ln^{3+} in which the energy transfer occurs to every intra-4f transition state of the doped Ln^{3+} ions, which is a little lower than the MLCT state of Sr_2CeO_4, after the nonradiative energy transfer from t_{1g}-f CTS to the MLCT state induced by the excitation in the CeO_6 groups, as shown by Figure 12.

Although the blue-white luminescence from Sr_2CeO_4 around 467 nm was severely quenched when Ln^{3+} ions were doped in Sr_2CeO_4, weak photoluminescence emission from Sr_2CeO_4 remained. The lifetimes of the luminescence at $\lambda_{em} = 467$ nm from Sr_2CeO_4:Ln^{3+} were found to be decreased drastically from that from Sr_2CeO_4 for all of Ln^{3+} employed, as shown in Figure 9b, and $\tau = 14$ μs for Eu^{3+}, 13 μs for Ho^{3+}, 22 μs for Tm^{3+}, and 16 μs for Er^{3+}. Sankar et al.[18] reported that the energy transfer from Ce^{4+} to Eu^{3+} was probably due to exchange interactions, because Sr_2CeO_4 has a one-dimensional structure with a short interchain distance of 3.597 Å (*c*-lattice parameter). This distance seems to be short enough for the energy transfer from the triplet state of MLCT to Ln^{3+} doped in the lattice. This energy transfer mechanism is likely to be similar to that from the triplet-excited state of aromatic compounds adsorbed into zeolite to the intra-4f excited state of Tb^{3+}, which is also immobilized into zeolite by cation exchange.[28] The decrease in lifetime of the CT emission from Sr_2CeO_4 by Ln^{3+} doping is therefore attributable to the direct energy transfer from the triplet excited state of the MLCT state to the intra-4f excited state of the Ln^{3+} ions.

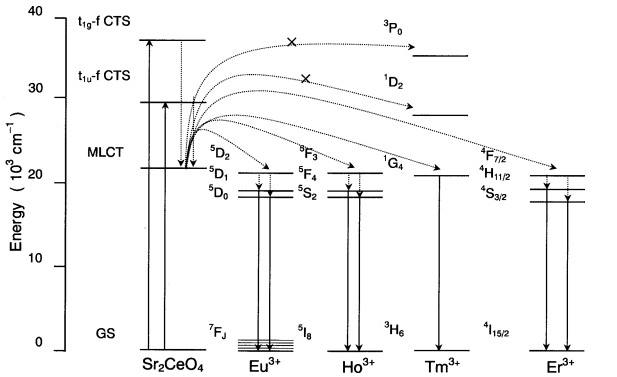

Figure 12. Schematic illustration of the energy diagram for Sr_2CeO_4:Ln^{3+} (Ln = Eu, Ho, Tm, and Er).

Conclusions

Sr_2CeO_4 blue phosphor particles were prepared by using an emulsion liquid membrane (ELM) system. The composite oxalate particles obtained were submicrometer size and much smaller than those prepared in the homogeneous aqueous solutions. Calcination of the composite oxalate particles at 1273 K gave submicrometer-sized Sr_2CeO_4 particles. The photoluminescence intensity of Sr_2CeO_4 particles prepared in the ELM system was comparable to that prepared by the solid-state method with longer time calcination.

We have also investigated the properties of Sr_2CeO_4 as a multiccolor phosphor by doping Ln^{3+} ions. In particular, Sr_2CeO_4:Eu^{3+} showed various emission spectra by changing the concentration of Eu^{3+}; the emission assigned to the $^5D_2$-$^7F_0$ transition was observed when the concentration of Eu^{3+} was low, and white luminescence was observed from the Sr_2CeO_4:Eu^{3+} particles. The lifetime corresponding to CT (charge-transfer) emission from Sr_2CeO_4 was decreased when the Ln^{3+} ions were doped, which was caused by the energy transfer from the triplet excited state of the MLCT (metal-to-ligand CT) state to the intra-4f excited state of the Ln^{3+} ions.

Acknowledgment. The authors are grateful to Mr. Masao Kawashima of the Gas Hydrate Analyzing System (GHAS), Osaka University for his experimental assistance in the characterization of the particles with SEM, and to the Division of Chemical Engineering for the Lend-Lease Laboratory Systems. The authors are also grateful to the Ministry of Education, Culture, Sports, Science and Technology, Japan (MEXT) for the financial support through the Grant-in-Aids for Scientific Research (No. 13650813) and Scientific Research on Priority Areas (417) "Fundamental Science and Technology of Photofunctional Interfaces" (No. 15033244), and to the New Energy

and Industrial Technology Development Organization (NEDO) for financial support through the Nanotechnology Materials Program—Nanotechnology Particle Project based on funds provided by Ministry of Economy, Trade and Industry, Japan (METI).

References and Notes

(1) Hirai, T.; Okamoto, N.; Komasawa, I. *AIChE J.* **1998**, *44*, 197−206.
(2) Hirai, T.; Okamoto, N.; Komasawa, I. *J. Chem. Eng. Jpn.* **1998**, *31*, 474−477.
(3) Hirai, T.; Okamoto, N.; Komasawa, I. *Langmuir* **1998**, *14*, 6648−6653.
(4) Hirai, T.; Hariguchi, S.; Komasawa, I.; Davey, R. J. *Langmuir* **1997**, *13*, 6650−6653.
(5) Hirai, T.; Kobayashi, J.; Komasawa, I. *J. Chem. Eng. Jpn.* **1998**, *31*, 787−794.
(6) Hirai, T.; Kobayashi, J.; Komasawa, I. *Langmuir* **1999**, *15*, 6291−6298.
(7) Hirai, T.; Hirano, T.; Komasawa, I. *J. Mater. Chem.* **2000**, *10*, 2306−2310.
(8) Hirai, T.; Hirano, T.; Komasawa, I. *J. Colloid Interface Sci.* **2002**, *253*, 62−69.
(9) Hirai, T.; Orikoshi, T.; Komasawa, I. *Chem. Mater.* **2002**, *14*, 3576−3583.
(10) Hirai, T.; Orikoshi, T. *J. Colloid Interface Sci.* **2004**, *269*, 103−108.
(11) Studenikin, S. A.; Cocivera, M. *Thin Soild Films* **2001**, *394*, 264−271.
(12) Kang, Y. C.; Park, S. B.; Lenggoro, I. W.; Okuyama, K. *J. Electrochem. Soc.* **1999**, *146*, 2744−2747.
(13) Lee, R. Y.; Kim, S. W. *J. Lumin.* **2001**, *93*, 93−100.
(14) Danielson, E.; Devenney, M.; Giaquinta, D. M.; Golden, J. H.; Haushalter, R. C.; McFarland, E. W.; Poojary, D. M.; Reaves, C. M.; Weinberg, W. H.; Wu, X. D. *Science* **1998**, *279*, 837−839.
(15) van Pieterson, L.; Soverna, S.; Meijerink, A. *J. Electrochem. Soc.* **2000**, *147*, 4688−4691.
(16) Park, C.-H.; Kim, C.-H.; Pyun, C.-H.; Choy, J.-H. *J. Lumin.* **2000**, *87−89*, 1062−1064.
(17) Nag, A.; Narayanan Kutty, T. R. *J. Mater. Chem.* **2003**, *13*, 370−376.
(18) Sankar, R.; Subba Rao, G. V. *J. Electrochem. Soc.* **2000**, *147*, 2773−2779.
(19) Eroglu, I.; Kalpakci, R.; Gunduz, G. *J. Membr. Sci.* **1993**, *80*, 319−325.
(20) Masui, T.; Chiga, T.; Imanaka, N.; Adachi, G. *Mater. Res. Bull.* **2003**, *38*, 17−24.
(21) Jiang, Y. D.; Zhang, F.; Summers, C. J.; Wang, Z. L. *Appl. Phys. Lett.* **1999**, *74*, 1677−1679.
(22) Sandhage, K. H. *Ceram. Trans.* **1997**, *85*, 103−126.
(23) Nakazawa, E. *Chem. Phys. Lett.* **1978**, *56*, 161−163.
(24) Nakazawa, E. *J. Lumin.* **1979**, *18/19*, 272−276.
(25) Tanabe, S.; Hirao, K.; Soga, N. *J. Non-Cryst. Solids* **1992**, *142*, 148−154.
(26) Guyot, Y.; Moncorge, R.; Merkle, L. D.; Pinto, A.; McIntosh, B.; Verdun, H. *Opt. Mater.* **1996**, *5*, 127−136.
(27) Yamamoto, H.; Mikami, M.; Shimomura, Y.; Oguri, Y. *J. Lumin.* **2000**, *87−89*, 1079−1082.
(28) Hashimoto, S.; Kirikae, S.; Tobita, S. *Phys. Chem. Chem. Phys.* **2002**, *4*, 5856−5862.